JOURNAL OF GEOPHYSICAL RESEARCH, VOL. 112, D16110, doi:10.1029/2007JD008519, 2007

A role for tropical tropospheric temperature adjustment to El Niño–Southern Oscillation in the seasonality of monsoonal Indonesia precipitation predictability

A. Giannini,[1] A. W. Robertson,[1] and J.-H. Qian[1]

Received 6 February 2007; revised 11 May 2007; accepted 30 May 2007; published 28 August 2007.

[1] We describe the seasonality in the variability and predictability of Indonesian monsoonal climate, dominated by the El Niño–Southern Oscillation (ENSO) phenomenon, and interpret it in light of theories of the development of the global ENSO teleconnection which explain the evolution of the response of the tropical ocean-atmosphere to ENSO's perturbation. High predictability during the dry and transition seasons, which coincide with ENSO growth, is expected from the coherent large-scale response to ENSO's initial perturbation. As the tropical ocean-atmosphere equilibrates to ENSO, and ENSO itself begins to decay, its direct influence diminishes, and regional features associated with the delayed response to ENSO become more prominent. Consistent with this interpretation, in a preliminary observational analysis of station data over Jawa we find that predictability is high during the growth phase of ENSO. We also find that at these regional scales there may be more predictability than previously thought as ENSO decays. Finally, we show that a simple one-tier prediction system, i.e., a system where the evolution of oceanic and atmospheric anomalies is internally consistent, better captures the intrinsic coupled nature of the ENSO teleconnection, compared to a two-tier system where the ocean forces the atmosphere, but does not respond to its feedback.

Citation: Giannini, A., A. W. Robertson, and J.-H. Qian (2007), A role for tropical tropospheric temperature adjustment to El Niño–Southern Oscillation in the seasonality of monsoonal Indonesia precipitation predictability, *J. Geophys. Res.*, *112*, D16110, doi:10.1029/2007JD008519.

1. Introduction

[2] At the crossroads between the region of warm sea surface temperature and high precipitation known as the Western Pacific warm pool, and the path of annual migration of the Asian-Australian monsoon [*Chang*, 2005], Indonesia is endowed with a warm and wet tropical climate. Traditional agricultural production systems are finely tuned to the local climate. The expectation for a certain amount of precipitation to accumulate on average during a certain period of the year, accompanied by a certain range in temperature, number of sunny days, or subseasonal distribution of rain events, etc. determines what type of production system is feasible at any one location.

[3] Seasonality, i.e., the contrast between warm and cold, wet and dry seasons, is spatially varied. In Indonesia it is less pronounced in equatorial regions than it is farther away from the equator (Figure 1 (all observational data sets used in this study are publicly available and can be downloaded from the IRI Data Library, http://iridl.ldeo.columbia.edu); also see *Aldrian and Susanto* [2003] for a classification of Indonesian climates). Over the islands of Jawa and Bali, and the island chain that comprises the Indonesian provinces of Nusa Tenggara Barat and Nusa Tenggara Timur and the sovereign nation of Timor Leste, the climate is monsoonal; that is, it is customary to distinguish a wet season (the Indonesian Bureau of Meteorology and Geophysics (BMG) classifies a month as belonging to the wet season when at least 150 mm are accumulated) from predominantly dry, fair-weather conditions during the rest of the year. The length of the wet season depends on the migration of the Asian-Australian monsoon [*Chang*, 2005], which is forced by the seasonal cycle in insolation through the response in land/ocean surface temperatures. This cycle follows a northwest to southeast track, such that the wet season is typically shorter the farther one moves away from the equator, i.e., considerably shorter over Timor than over Jawa.

[4] However, how likely is it that the average expected climate will be realized year after year? How ample a deviation from the climatological mean is it reasonable to expect, and with what frequency? What is of interest in the study of climate variability and its predictability is to diagnose how a season or month in a specific year deviated, or to prognose how likely it is to deviate from the mean

[1]International Research Institute for Climate and Society, Earth Institute, Columbia University, Palisades, New York, USA.

0148-0227/07/2007JD008519$09.00

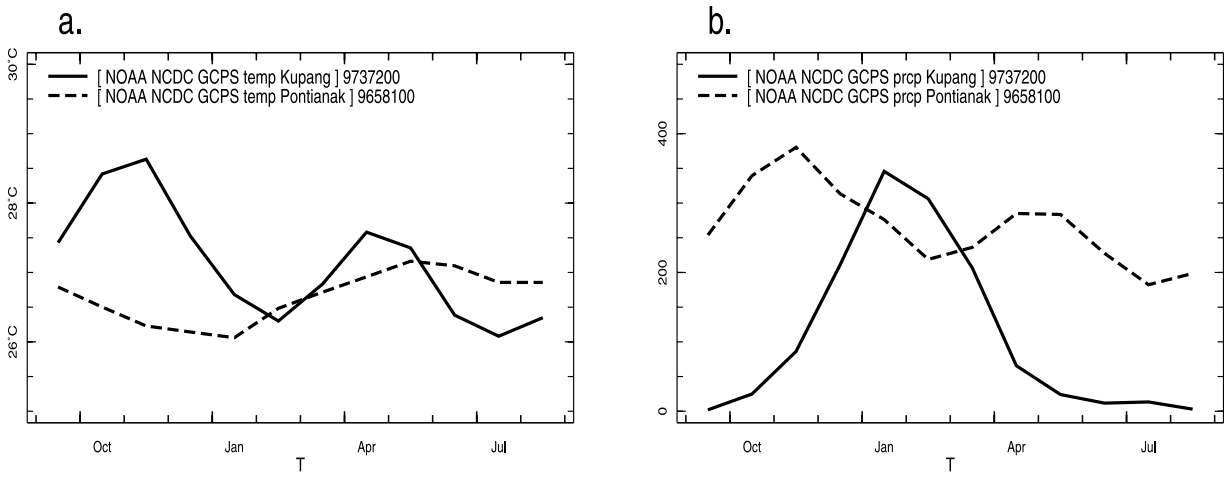

Figure 1. Seasonal cycles of (a) temperature and (b) precipitation at two sites in Indonesia. One is Pontianak, in West Kalimantan (0.15°S, 109.4°E; dashed lines), representative of the equatorial climate type. The other is Kupang, in Nusa Tenggara Timur (10.17°S, 123.67°E; solid lines), representative of the monsoonal climate type. Data are from NOAA's National Climate Data Center/Global Climate Perspectives System (GCPS).

climatological expectation. In the following, we summarize aspects of the predictability of Indonesian climate as they relate to the El Niño–Southern Oscillation (ENSO). Focusing on the island chain from Jawa to Timor, which we loosely describe as being part of "monsoonal Indonesia," we propose an explanation for the observation that predictability is high during the dry and transition seasons, but low during the core monsoon season, when patterns of variability lack large-scale coherence. We refer to this behavior as "seasonality in the predictability of precipitation." This explanation hinges on recent theoretical and modeling studies by Chiang and collaborators and Neelin and collaborators that explain the development of a new quasi-equilibrium state in the global tropical ocean-atmosphere system, a state that is attained in response to ENSO in the seasons immediately following mature conditions in the equatorial Pacific Ocean.

[5] Related work accomplished in the framework of a project funded by the U.S. Agency for International Development (USAID)'s Office of Foreign Disaster Assistance on "Climate forecast applications for disaster mitigation" is detailed in companion papers by J.-H. Qian et al. (A dipolar pattern of precipitation anomaly over Java Indonesia associated with El Niño, manuscript in preparation, 2007, hereinafter referred to as Qian et al., manuscript in preparation, 2007), on dynamical downscaling using a regional model, and V. Moron and A. W. Robertson (Spatial coherence and intra-seasonal variability of Indonesian rainfall: Preliminary results, manuscript in preparation, 2007), on statistical downscaling to subseasonal timescales.

2. ENSO: Source of Predictability for Indonesia

[6] As indicated by many studies focusing on the relationship between sea surface temperature (SST) and the climate of Indonesia [e.g., *Hackert and Hastenrath*, 1986; *Harger*, 1995; *Kirono et al.*, 1999; *McBride et al.*, 2003; *Aldrian and Susanto*, 2003; *Chang et al.*, 2004] the dominant source of year-to-year variability in Indonesian climate is the El Niño–Southern Oscillation (ENSO) phenomenon, the most influential climate pattern globally at interannual timescales [*Ropelewski and Halpert*, 1987; *Wallace et al.*, 1998]. The impact of ENSO on precipitation is depicted in Figure 2. The two panels represent anomalies typical of the warm and cold phases of ENSO, also known respectively as El Niño and La Niña. 12-month mean anomalies are computed from July of the year of ENSO onset, or year(0) (onset typically occurs during the transition between wet and dry Southern Hemisphere monsoon seasons) to the June of the following year, or year(1), by which time the ENSO event has usually ended [*Rasmusson and Carpenter*, 1982]. The Indonesian/Maritime continent/Western Pacific warm pool region is at the center of the phenomenon. In the warm ENSO case, negative precipitation anomalies develop over the Western Pacific warm pool as deep convection and precipitation shift eastward toward the central and eastern equatorial Pacific. In contrast, the cold ENSO case is to a large extent appropriately described as an enhancement of climatological conditions, i.e., heavier than normal precipitation over the climatologically wet Western Pacific warm pool, and enhanced dryness over the climatologically dry cold tongue of the central and eastern equatorial Pacific.

[7] Maximum precipitation anomalies around the international dateline (positive in the warm ENSO case, negative in the cold ENSO case (in Figure 2)) are not exactly colocated. They are just to the east of it in the warm ENSO case, just to the west in the cold ENSO case. Such nonlinearities in the ENSO system have been investigated in relation to their effect on variability in the Northern Hemisphere midlatitudinal response to ENSO [e.g., *Hoerling et al.*, 1997]. In this paper we choose to focus our analysis on warm ENSO events. The reader is referred to, e.g., *Ropelewski and Halpert* [1989] for a global survey of canonical La Niña rainfall anomaly patterns.

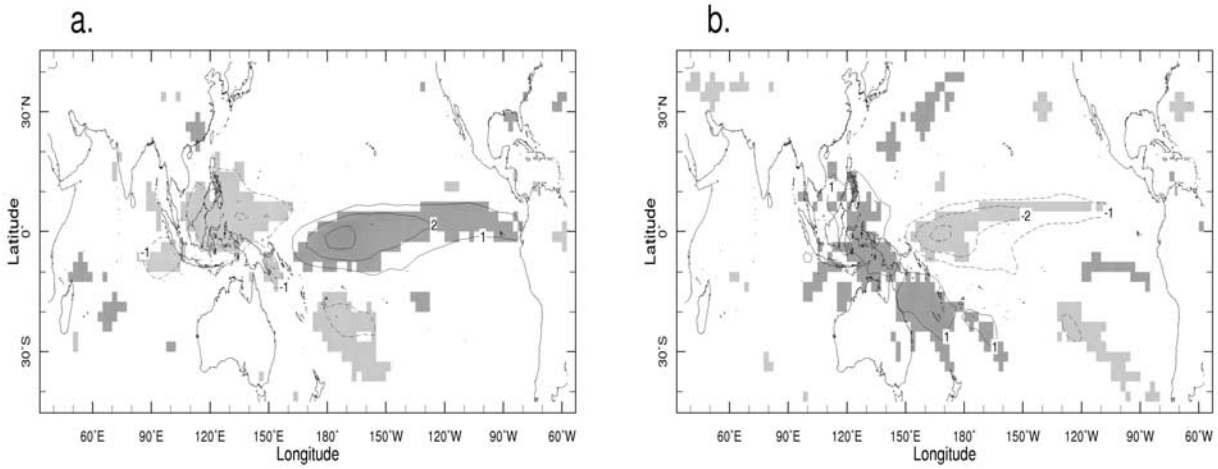

Figure 2. Composite anomalies in precipitation typical of (a) warm and (b) cold ENSO events. Data are from the Global Precipitation Climatology Project (GPCP [*Huffman et al.*, 1997]). Anomalies are averaged over the ENSO year from July of year(0) to June of year(1). Warm and cold ENSO events are identified on the basis of the December(0)–January(1) value of Niño3.4 being greater than 1°C or less than −1°C, respectively. In 1979–2005 there were six warm and four cold events. Anomalies are every mm/day; dashed indicates negative and solid indicates positive. The shading, light for negative anomalies and darker for positive anomalies, represents statistical significance of the anomalies with respect to climatology, at the 5% confidence level or greater, based on a two-sided t-test.

[8] Inception of an ENSO event in the central equatorial Pacific is brought about by the dynamical coupling of atmosphere and ocean that gives rise to local anomalies, e.g., in precipitation, near-surface winds, surface temperature and ocean heat content that grow, reach maturity, start decaying, and sometimes reverse in an internally consistent way (see, e.g., *Neelin et al.* [1998] for a review). Here we present evidence that the development that follows, of global anomalies in the atmosphere and oceans known as teleconnections [*Ropelewski and Halpert*, 1987; *Glantz et al.*, 1991; *Wallace et al.*, 1998], can be interpreted as an adjustment process to the perturbation initiated by tropical Pacific anomalies. Central to our dynamical interpretation of ENSO's impact on Indonesia is the observation that anomalies, especially tropical atmospheric anomalies, are larger from ENSO onset to maturity, i.e., during the first half of a typical ENSO life cycle, which coincides with the second half of the year(0) calendar year, and that as ENSO starts to decay in the first half of year(1), the climate system in and around Indonesia behaves as if it had reached a new equilibrium, the result of having adjusted to ENSO's jolt. In other words, the global-scale pattern of influence breaks down, and the spatial coherence of ENSO's regional effects is largely reduced. Climatologically speaking, July–December spans the dry and transition seasons in Indonesia, while January–June includes the core Southern Hemisphere summer monsoon season of January–March (Figure 3).

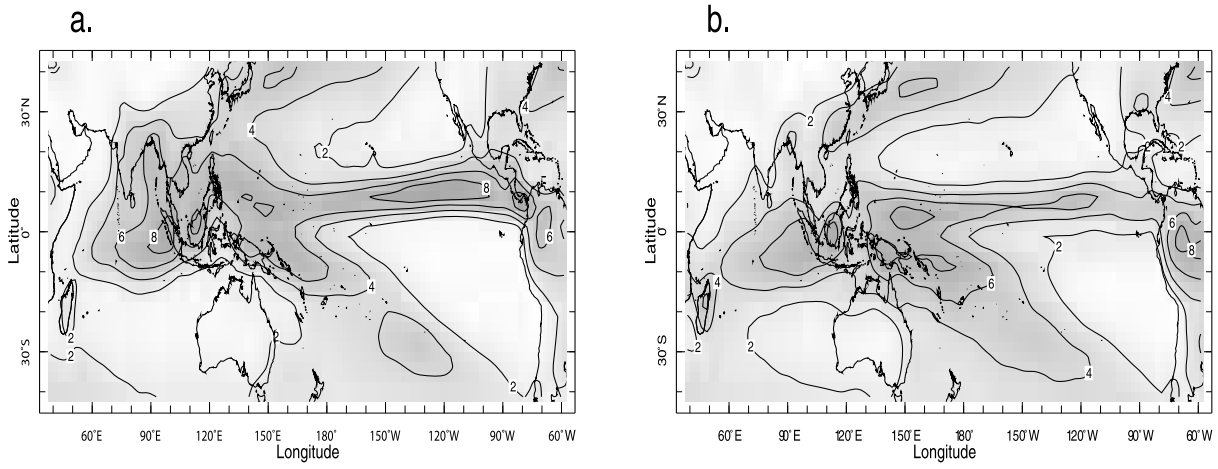

Figure 3. Seasonal climatology of rainfall, in (a) July–December and (b) January–June, from GPCP, as in Figure 2. Contour is every 2 mm/day, and darker shading indicates higher rainfall rates.

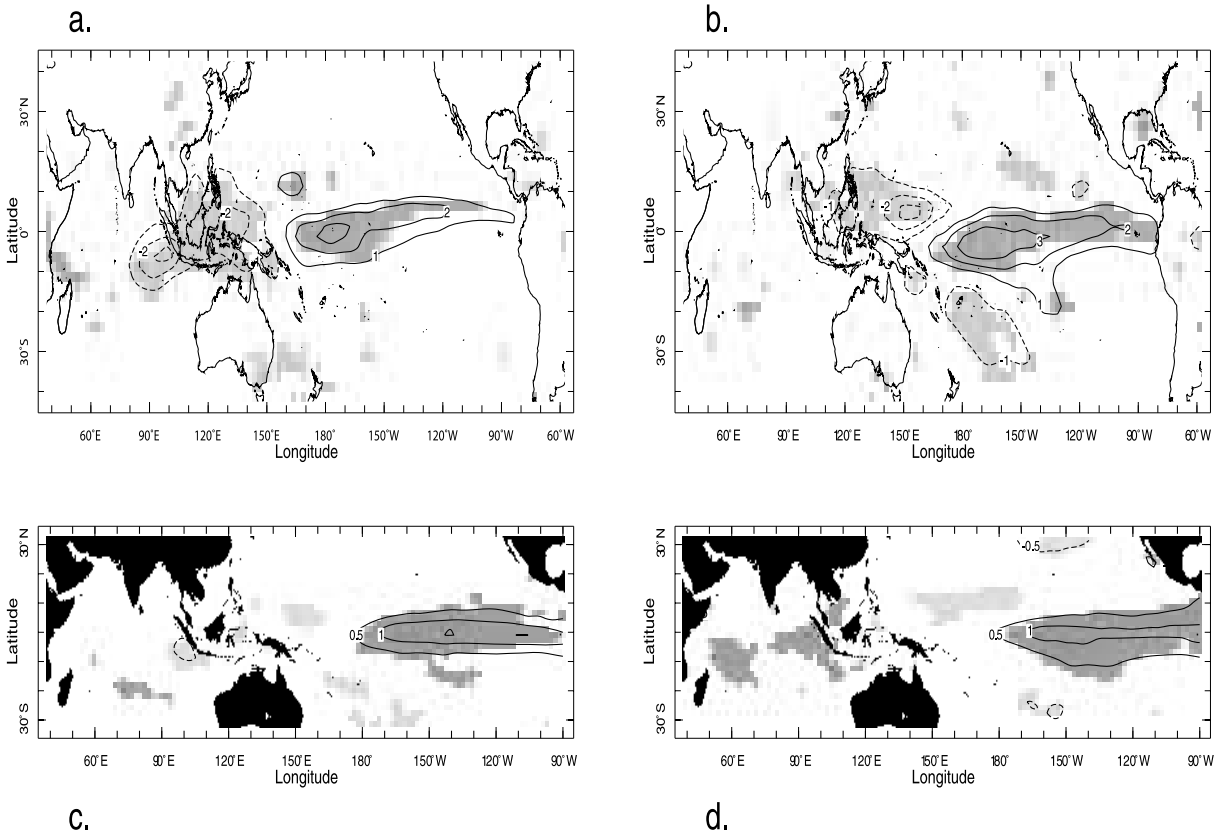

Figure 4. Composite anomalies in (a and b) precipitation and (c and d) sea surface temperature (SST) during warm ENSO events in 1979–2005. Precipitation is from GPCP, as in Figures 2 and 3. SST is from the NCEP-NCAR Reanalysis [*Kalnay et al.*, 1996]. In Figures 4a and 4c, anomalies are averaged over the first half of an ENSO year, from July to December of year(0). In Figures 4b and 4d, they are averaged over the second half, from January to June of year(1). Warm ENSO events are identified as in Figure 2. Contour is every mm/day for precipitation, every 0.5°C for SST; solid indicates positive and dashed indicates negative anomalies. The shading, light and darker for negative and positive anomalies, respectively, represents statistical significance of the anomalies with respect to climatology, at the 5% confidence level or greater, based on a two-sided t-test.

[9] Consistent with this interpretation, when the ENSO year of Figure 2 is broken into two 6-month periods, namely July to December of year(0), and January to June of year(1), shown in Figure 4 in the averages of El Niño cases, it is found that the significant precipitation anomalies over monsoonal Indonesia typical of July–December(0) vanish in January–June(1). Hence, from this viewpoint, predictability as defined by ENSO can be expected to be high in July–December(0), and low in January–June(1) [*Aldrian et al.*, 2007]. SST anomalies (Figures 4c and 4d) in the ENSO source region of the tropical Pacific grow and peak in July–December(0). In contrast, SST anomalies opposite in sign to those in the source Pacific region initially develop in the Western Pacific warm pool and eastern Indian Ocean, but later reverse to the same sign as in the source region, continuing to develop into January–June(1).

[10] The key question that this study addresses is why this behavior in the life cycle of ENSO-related anomalies in monsoonal Indonesia; specifically, why coherent large-scale precipitation anomalies at the end of year(0), but not during the core of the monsoon, at the beginning of year(1)? As depicted in Figure 5, the near-surface circulation is remarkably consistent in transitioning from July–December of year(0) to January–June of year(1): Divergence dominates over the Maritime continent, with easterly anomalies in the Indian Ocean sector, and westerly anomalies in the Pacific Ocean sector. Why, then, are precipitation anomalies not consistent in both seasons?

3. ENSO's Impact on the Maritime Continent: Large-Scale View

[11] The global atmosphere responds quickly to the perturbation imposed by the shift in precipitation in the equatorial Pacific Ocean; during a warm ENSO the entire tropical troposphere warms up [*Yulaeva and Wallace*, 1994; *Su et al.*, 2005; *Lintner and Chiang*, 2007]. Surface temperatures take more time to equilibrate to the warming of the atmosphere [*Klein et al.*, 1999; *Chiang and Sobel*, 2002; *Chiang and Lintner*, 2005]. For as long as the imbalance persists between surface and atmospheric temperatures above the planetary boundary layer, a warm ENSO translates into a more stable atmospheric vertical profile, unfavorable for deep convection and precipitation, hence the widespread tropical dry anomalies. Then, as surface temperatures adjust to the warmer troposphere, a new "equi-

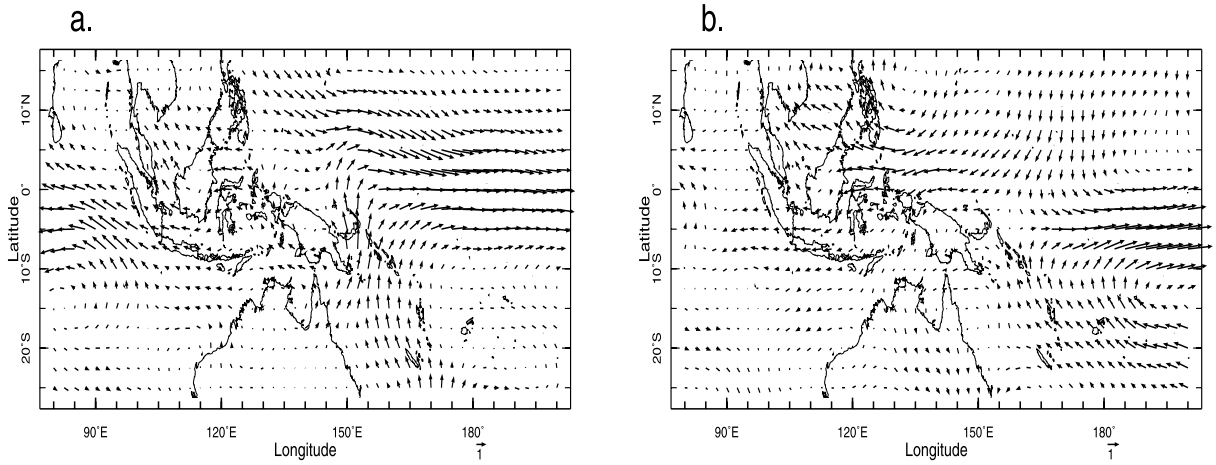

Figure 5. Composite anomalies in 1000 hPa winds during warm ENSO events in 1949–2005. (a) July–December of year (0) and (b) January–June of year(1).

librium'' is found. We use the quotation marks here, because strictly speaking it is not correct to speak of ''equilibrium''; the ENSO system grows and then decays, never reaching a steady state. However, here we wish to stress the difference between the growth phase of ENSO, when the global tropical system is perturbed and responds with large-scale coherence, and the following phase, when the system response loses coherence. In addition, how this equilibrium manifests itself locally depends on the details, on the mechanisms by which near-surface humidity adjusts to free-tropospheric temperature, e.g., through changes in evaporation and moisture convergence [*Su and Neelin*, 2002; *Lintner and Chiang*, 2007]. The end result is that the absence of coherent large-scale forcing in the ENSO decay phase allows for conditions that have developed locally in relation to ENSO to take hold. As we will see in section 4 (also see Qian et al., manuscript in preparation, 2007), these can favor or hinder deep convection locally.

[12] In the following subsections we describe in greater detail ENSO-related anomalies in the global tropical atmospheric circulation, and in the evolution of SST around Indonesia.

3.1. ENSO-Induced Atmospheric Anomalies in the Indo-Pacific Sector

[13] The large-scale atmospheric circulation associated with growth/mature and decay phases of a warm ENSO event is described in Figure 6. Figures 6a and 6b depict the velocity potential at 200 hPa. Figures 6c and 6d depict vertical velocity at 500 hPa. Figures 6e and 6f depict sea level pressure. The contrast between July–December(0) and January–June(1) pictures is easy to notice. In July–December(0) (Figures 6a, 6c, and 6e) the equatorial belt in the Indo-Pacific sector is clearly the focus of action. Centers of action can be recognized over the Maritime continent and in the central Pacific. Centers of anomalously positive and negative velocity potential at 200 hPa broadly define the location of anomalous convergence and divergence at upper levels. At middle levels, these same centers of convergence and divergence are associated with subsidence and ascent, respectively. The surface expression of this large-scale circulation pattern is the Southern Oscillation; anomalously high sea level pressure over the Western Pacific, Maritime continent and tropical Oceania, and anomalously low sea level pressure in the central and eastern equatorial Pacific. In the Southern Hemisphere, a wave train known as the Pacific–South American pattern [*Mo and Higgins*, 1998] emanates from the Maritime continent and arches eastward, first poleward and then equatorward, into the South Atlantic.

[14] In January–June(1) (Figures 6b, 6d, and 6f) action in the central equatorial Pacific has largely subsided. Though residual anomalies remain over the Western Pacific warm pool, the focus has now shifted to the Northern Hemisphere subtropics, as exemplified in both upper level velocity potential and sea level pressure. Again, a wave train, known as the Pacific–North American (PNA [*Wallace and Gutzler*, 1981]) pattern, is visible in sea level pressure.

[15] Anomalies in the vertical temperature profiles during the growth and decay phases of ENSO are depicted in Figure 7, for the core ENSO region (180–240°E, 15°S–15°N; Figures 7a and 7b) and the Maritime continent (100°E–160°E, 15°S–15°N; Figures 7c and 7d). These correspond to the regions of enhanced ascent and subsidence, respectively, in the July–December(0) panel of vertical velocity, in Figure 6c. In July–December(0) the temperature profile below 700 hPa is unstable in the core ENSO region, stable over the Maritime continent, as expected. Over the Maritime continent, temperature anomalies start on the negative side at the surface, consistent with the cool SST anomalies there. The difference in stability is much amplified in the equivalent potential temperature (θ_e) profiles, implying a nonnegligible contribution from changes in humidity. This is also true in January–June(1), when the vertical profiles in θ_e become unstable in both regions below 850 hPa.

3.2. ENSO-Induced SST Anomalies in the Indonesian Seas

[16] The ENSO-related response of sea surface temperatures in basins remote from the tropical Pacific has been argued to come about both because of changes in thermodynamic and ocean dynamical forcings [*Klein et al.*, 1999; *Murtugudde et al.*, 2000]. Thermodynamic forcings include changes in radiation associated with cloud cover changes,

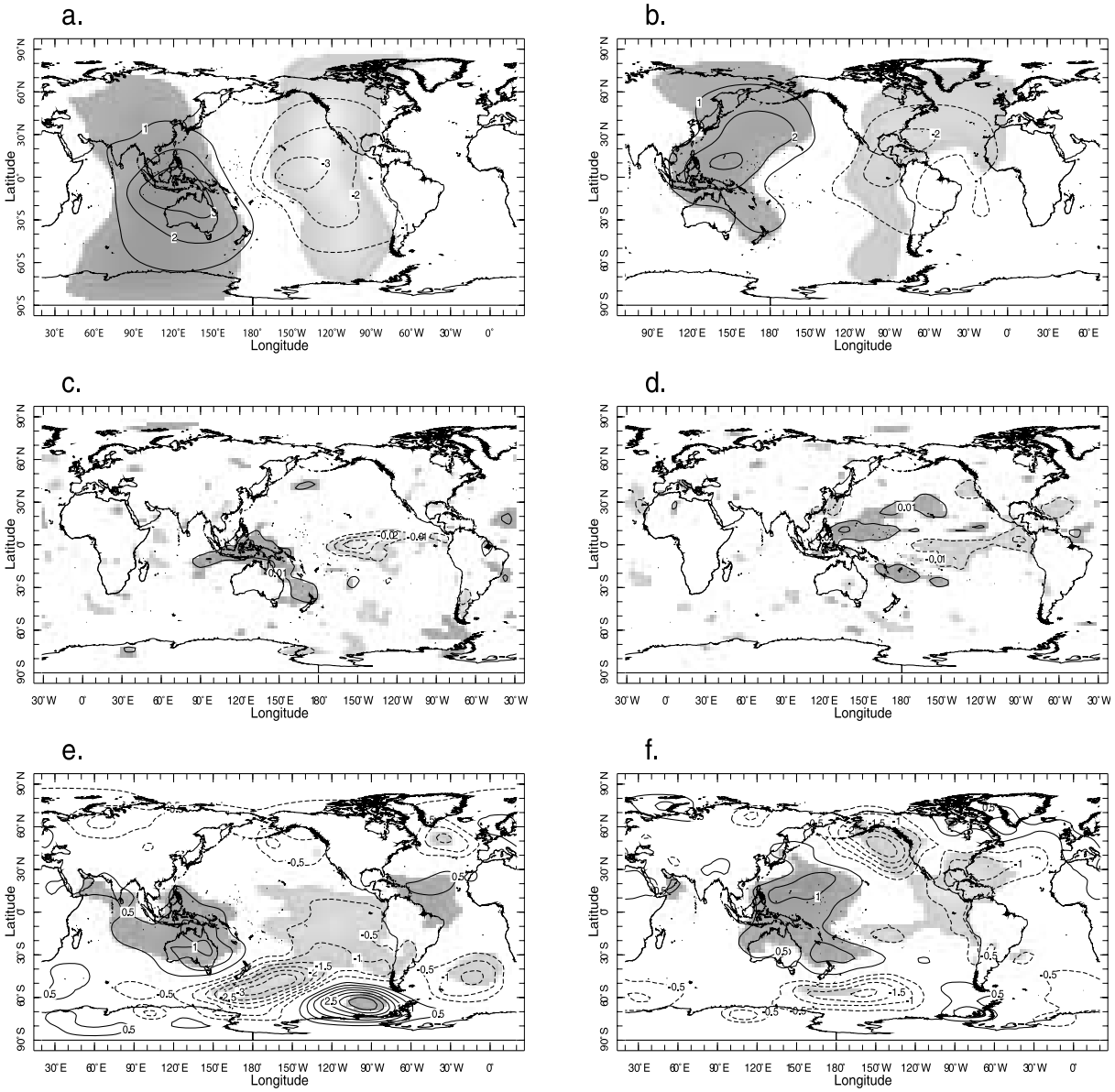

Figure 6. Composite warm ENSO anomalies with respect to neutral conditions in (a and b) velocity potential at 200 hPa, (c and d) pressure vertical velocity at 500 hPa (positive values indicate downward motion, or subsidence), and (e and f) sea level pressure. Figures 6a, 6c, and 6e are for July–December(0), and Figures 6b, 6d, and 6f are for January–June(1). Data are from the NCEP-NCAR Reanalysis over the period 1949–2005. During this period we identified 11 warm (and 9 cold) ENSO events on the basis of Niño3.4 being larger than 1°C (or less than −1°C) in December(0)–January(1). Shading represents statistical significance of the difference at the 5% confidence level, light for negative anomalies and darker for positive anomalies. The contour in velocity potential is every 1000000 m^2 s^{-1}, in pressure vertical velocity it is every 0.01 Pa/s, and in sea level pressure it is every 0.5 hPa.

and in evaporation, due both to changes in near-surface wind speed (e.g., *Hendon* [2003] in the case of the Maritime continent), and in the temperature difference between the ocean surface and the overlying atmospheric boundary layer (*Saravanan and Chang* [2000] in the case of the tropical Atlantic [*Chiang and Sobel*, 2002; *Chiang and Lintner*, 2005]). Ocean dynamical forcings include wind-driven changes in the depth of the equatorial thermocline and in coastal upwelling.

[17] Year(0) of a warm ENSO event is characterized by cold anomalies in surface temperature in the seas around Indonesia, an appendix of the boomerang-shaped anomalies of the same sign that surround the warming in the equatorial Pacific Ocean. These cold anomalies extend westward from the dateline into the Maritime continent and eastern Indian Ocean (Figure 3c). They are consistent with reduced trapping of long-wave radiation, as the high-level clouds associated with deep convection have migrated eastward

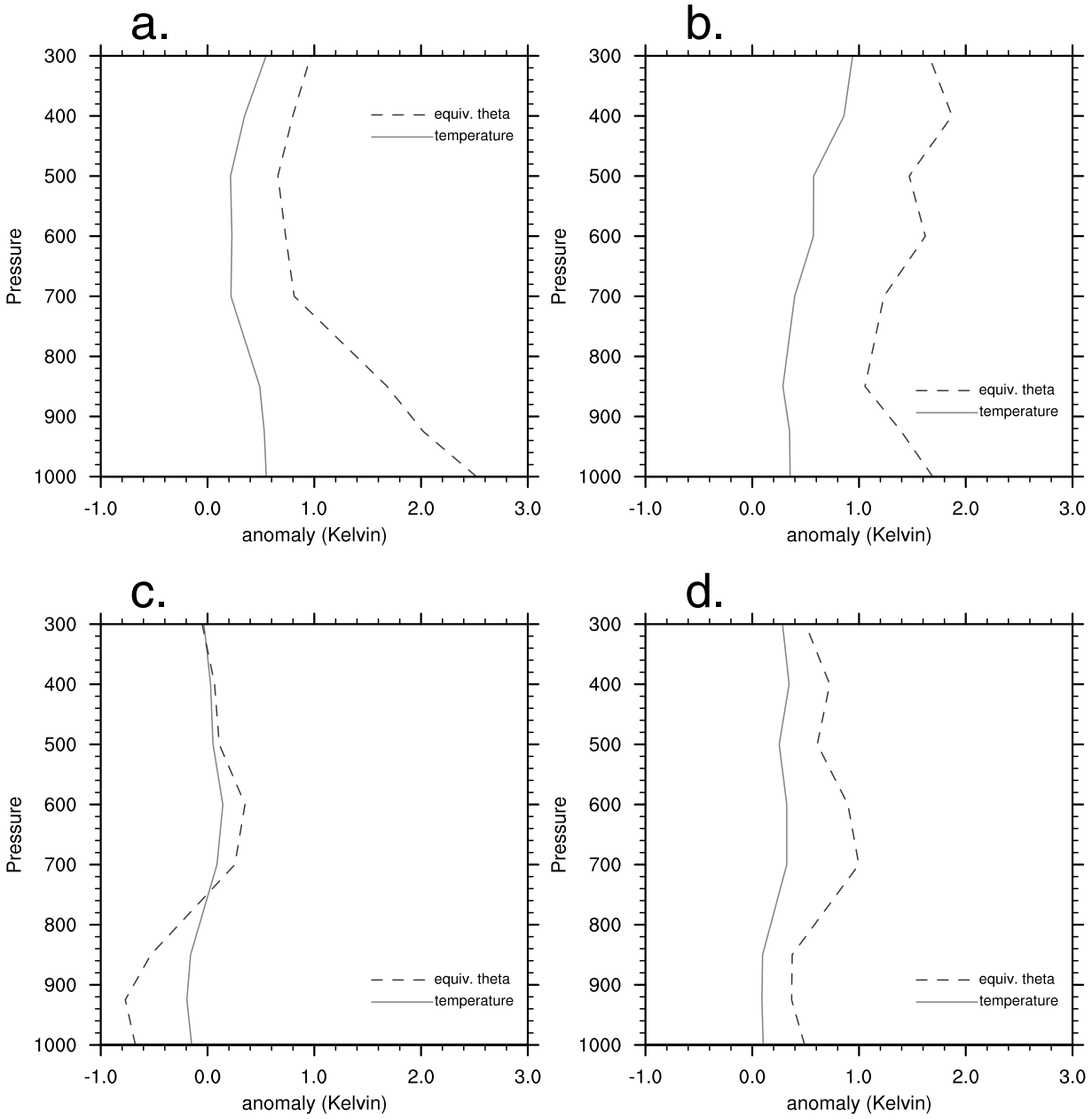

Figure 7. Vertical profiles of warm ENSO anomalies in temperature (solid) and equivalent potential temperature (dashed) in two regions: (a and b) the core ENSO central equatorial Pacific, between 180° and 240°E, 15°S and 15°N, and (c and d) the Maritime continent, between 100°E and 160°E, 15°S and 15°N.

into the central and eastern equatorial Pacific [*Park and Leovy*, 2004]. They are also consistent with near-surface easterly anomalies in the eastern Indian Ocean, which act to strengthen wind speed, hence increase evaporation and cooling [*Hendon*, 2003]. In places, such as the southern coasts of Sumatera and Jawa, these same easterly anomalies have an along-shore component that enhances coastal upwelling, further amplifying the negative anomalies [*Murtugudde et al.*, 2000; *Susanto et al.*, 2001]. The cold local SST anomalies contribute to making the overall vertical temperature profile even more stable from the bottom up (Figure 7c), reinforcing the negative precipitation anomalies around Indonesia.

[18] Then, in year(1), as monsoonal Indonesia enters the core of the wet season while ENSO is winding down, warm SST anomalies manifest themselves in the Indian Ocean and around the Western Pacific warm pool (Figure 3d). The warming is most conspicuous in the seas around Indonesia to the south of the equator; the SST tendency between October–December of year(0) and January–March of year(1), calculated in Wm^{-2} assuming a mixed layer h of constant depth of 50m in $\rho c_p h \frac{\partial To}{\partial t}$, is depicted in Figure 8a.

[19] To explain this development we first focus on the contribution of thermodynamic ocean-atmosphere interaction. Net heat flux into the surface (Figure 8b), the sum of latent and sensible heat fluxes, and radiation terms, is

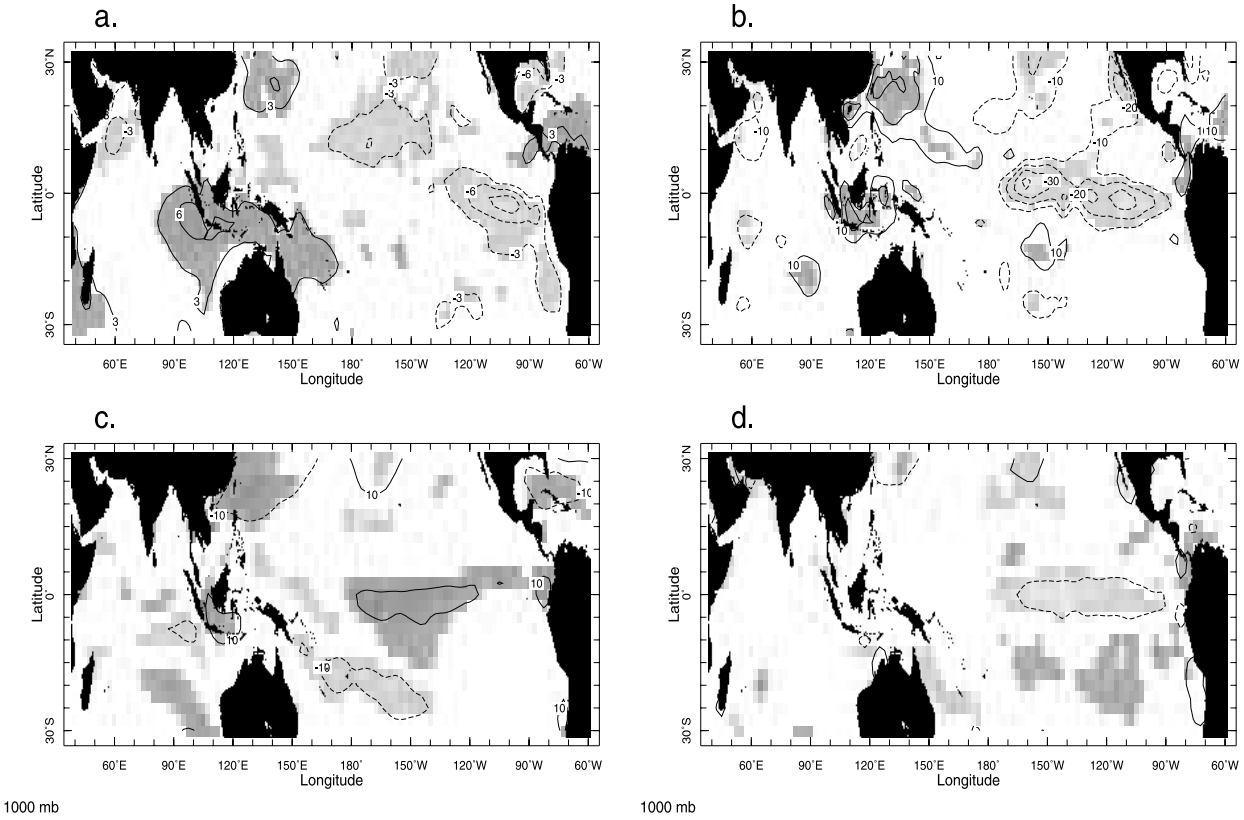

Figure 8. Composite warm ENSO anomalies with respect to neutral conditions of (a) the SST tendency between October–December of year(0) and January–March of year(1) and of thermodynamic terms influencing it (in W m^{-2}), (b) November(0)–February(1) average net heat flux anomalies (positive into the ocean), (c) net heat flux anomalies due to anomalies in wind speed, and (d) anomalies due to the atmosphere-ocean temperature difference (bottom right). In Figure 8c, because the climatological mean ($T_a - T_o$) is negative everywhere in the domain depicted, except for the eastern equatorial Pacific, where it is close to zero, positive anomalies represent negative wind speed anomalies and warming of the ocean's surface. In Figure 8d, negative anomalies represent a negative anomalous ($T_a - T_o$), i.e., an ocean surface warmer than the atmosphere immediately overlying it. Shading, dark for positive anomalies and lighter for negative anomalies, represents statistical significance of the anomalies at the 5% level. All data are from the NCEP-NCAR Reanalysis over 1949–2005.

positive in the Indonesian Seas. The dominant terms contributing to it are net solar radiation into the surface, which increases because of a decrease in cloud cover, and latent heat flux (not shown). To further diagnose evaporation, following *Saravanan and Chang* [2000] we linearize the bulk formula for the dependence of the net heat flux into the surface (F) on changes in wind speed (W) and in the atmosphere-ocean temperature difference (ΔT), and compute the anomalous fluxes, due to anomalous wind speed, and to anomalous atmosphere-ocean temperature difference, respectively as $F'_W = \frac{W'}{\overline{W}}\overline{F}$, and $F'_{\Delta T} = \frac{\Delta T'}{\overline{\Delta T}}\overline{F}$, where the $()'$ and $\overline{()}$ denote deviations from climatology and climatological values, respectively. These two terms are depicted in Figures 8c and 8d.

[20] The two mechanisms are very different in their spatial footprint. Changes in wind speed, with positive values implying an oceanic warming (Figure 8c; see the figure caption for a more detailed explanation), have a localized effect in the Indonesian Seas region; an area of reduced wind speed stands out in the longitudinal band between 100°E and 120°E, channeled between Sumatera and Kalimantan. In contrast, increased wind speed to the southeast of Sumatera and Jawa would be locally consistent with cooling, but such tendency is not apparent in SST, possibly because there has been no change compared to previous months. Changes in the atmosphere-ocean temperature difference (Figure 8d) are indicative of broad equilibrium conditions everywhere except where ocean dynamics plays a role, i.e., in the central and eastern equatorial Pacific, where large, negative anomalies represent the warming action exacted by the ocean on the overlying atmospheric boundary layer. Elsewhere, no significant anomalies can be noted, another telltale sign that the ocean's surface has adjusted to the warm ENSO-induced tropospheric warming on subseasonal timescales.

[21] The thermodynamic, ocean-atmosphere interaction terms just discussed cannot fully explain the broad spatial footprint of the pattern of warming tendency in the Indonesian Seas. The role of ocean dynamics in setting up SST anomalies in this region has also been analyzed, and found to be critical in connecting equatorial Pacific and Indian Ocean responses [*Wijffels and Meyers*, 2004; *Bracco et al.*, 2005, 2007]. This contribution is visible in Figure 8a. Near-surface wind anomalies typical of the growth phase of warm

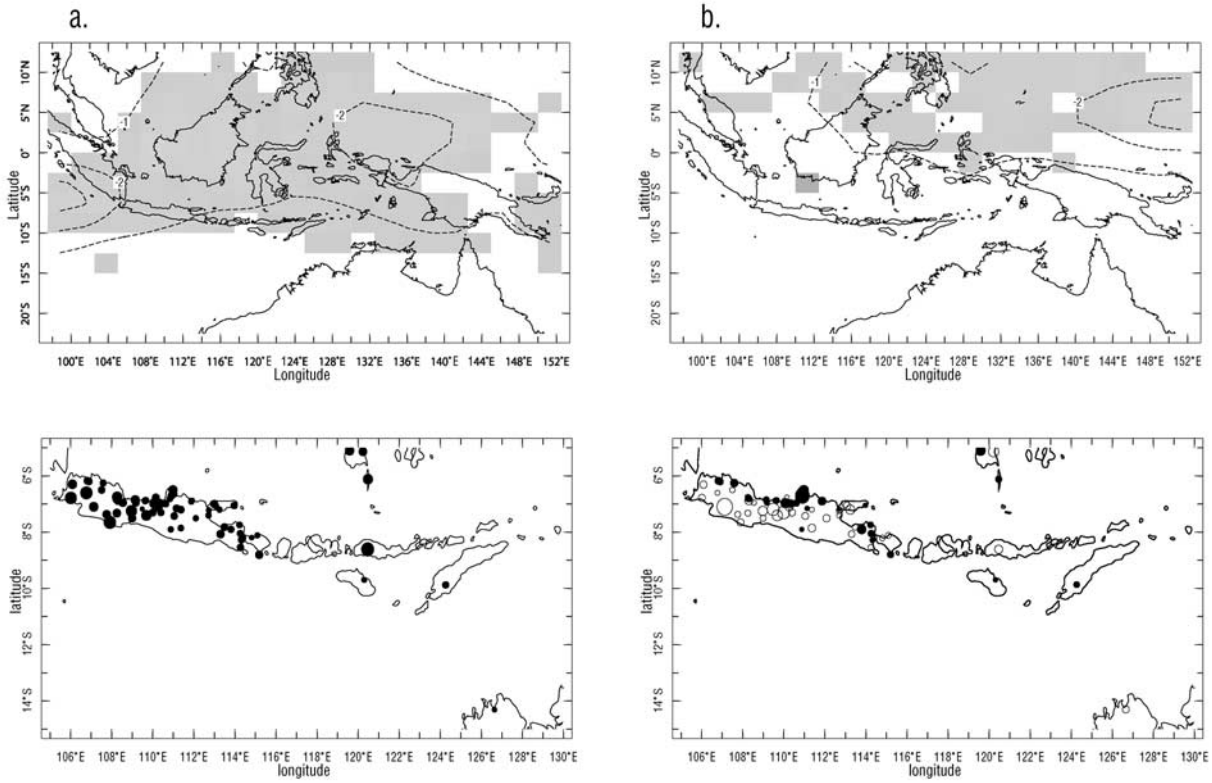

Figure 9. Composite anomalies in precipitation during (a) July–December(0) and (b) January–June(1) of warm ENSO events. The top row shows anomalies in the Indonesian region based on GPCP data, which covers the period 1979–2005; contours and shading are as in previous figures. The bottom row shows anomalies in station data at locations in the NOAA/NCDC/GHCN data set, composited over 1950–1975; solid circles are for negative anomalies, and open circles are for positive anomalies. There were five warm ENSO events in this earlier period, identified using the same technique as in previous figures.

ENSO, depicted in Figure 5a, with anomalous easterlies in the Indian Ocean, and anomalous westerlies in the Western Pacific Ocean, draw a divergent circulation around Indonesia. This anomalous near-surface wind pattern is consistent with the initial shoaling of the thermocline in the Indonesian Seas, possibly a component of the cooling of the Indonesian Seas in July–December(0) (see Figure 3c). The subsequent warming can be explained again in both thermodynamic and ocean dynamical terms. It may be that a shallower mixed layer warms up more easily to the increased solar radiation associated with decreased convection and cloud cover, or that equatorial ocean dynamics of the delayed oscillator type may play a role, not only in the tropical Pacific, but also in the Indian Ocean. Adjustment of the thermocline in the Indonesian Seas, triggered by the convergence of an eastward propagating Kelvin wave from the Indian Ocean and a westward propagating Rossby wave from the Pacific Ocean, both downwelling/warming, would also call for a delayed warming of the shallow seas around Indonesia [*Wijffels and Meyers*, 2004].

[22] In conclusion, despite its complexity, ENSO's impact on the Indo-Pacific sector as viewed from a large-scale perspective is sufficient to explain anomalies in the ocean-atmosphere system that have an effect on Indonesian precipitation. Next we investigate the regional-scale attributes of the latter.

4. ENSO's Impact on Monsoonal Indonesia: Regional View

[23] The contrast between the strength of ENSO's impact on monsoonal Indonesia precipitation toward the end of year(0) and its weakness at the beginning of year(1) had already been noted by *Haylock and McBride* [2001], among others. In Figure 9 we compare composite anomaly maps of the July–December(0) and January–June(1) warm ENSO seasons obtained from 2 precipitation data sets very different in character. One is that already used in Figures 2, 3, and 4, i.e., the NASA GPCP (Global Precipitation Climatology Project [*Huffman et al.*, 1997]) satellite-gauge product, which has global coverage, though at coarse (2.5° by 2.5°) spatial resolution, and is obtained by blending various satellite estimates of precipitation with rain-gauge data where available. The other is station data available from NOAA GHCN (Global Historical Climate Network [*Vose et al.*, 1992]).

[24] The GHCN stations were selected in the monsoonal Indonesia region, from Jawa to Timor, on the basis of completeness of their monthly precipitation records for the

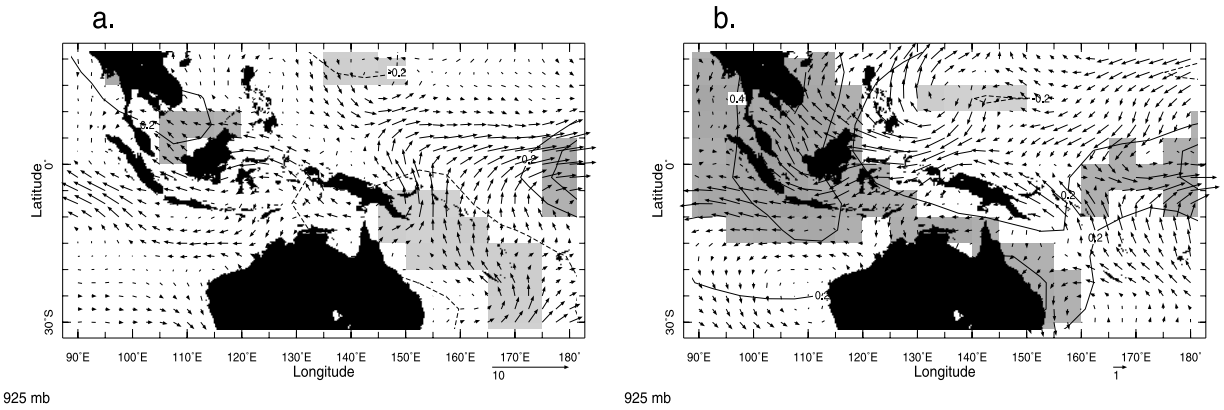

Figure 10. Composite anomalies in sea surface temperature, from *Kaplan et al.* [1997, 1998], and in NCEP-NCAR Reanalysis 925 hPa winds, during (a) July–December(0) and (b) January–June(1) of warm ENSO events in 1950–1975, i.e., the same years as in the bottom plots of Figure 9. Shading, in dark grey for positive SST anomalies and lighter gray for negative anomalies, represents statistical significance at the 5% level.

period with best coverage, which is 1950–1975. The July–December(0) anomaly plots compare favorably in the two data sets (Figures 9a and 9c), despite the fact that they were computed on nonoverlapping periods; the warm ENSO-related large-scale drying in GPCP translates into spatially coherent, below-average precipitation, the same at virtually all stations in GHCN. The more interesting feature emerges in the January–June(1) plots (Figures 9b and 9d). Here, the lack of spatial coherence at the large-scale (no significant anomaly is present in the GPCP plot over monsoonal Indonesia (Figure 9b)) translates into a dipole pattern over Jawa (Figure 9d), with continued drying along the northern coast, and a reversal of anomalies with respect to the previous season everywhere else. Data from other islands is too scarce to arrive at any conclusion.

[25] The higher degree of spatial detail in the January–June(1) station composite compared to the homogeneous below-average conditions in the July–December(0) composite points to the emergence of local forcings. It seems reasonable to infer that as the large-scale picture dictated by ENSO has slowly evolved into a new thermodynamic equilibrium, local dynamical features, such as topography or regional gradients in sea surface temperature may take control. The general conditions that accompany this development locally are depicted in Figure 10; in January–June(1) (Figure 10b) SST anomalies in the eastern Indian Ocean and around the Maritime continent have reversed in sign, as discussed earlier. Near-surface winds anomalies are easterly, and stronger north of Jawa than in the open Indian Ocean to its south.

[26] The specific conditions that explain the rainfall dipole over Jawa require the dynamical interpretation of these easterly anomalies in the context of the mean climatological westerly winds typical of the monsoon season. In this context, easterly anomalies translate into weaker winds. If one imagines that the near-surface flow is further slowed down over Jawa compared to over the surrounding seas, because of enhanced friction over land, the configuration that results from these easterly anomalies is one of positive northward shear in the zonal wind component, which translates into clockwise vorticity and divergence, hence reduced rainfall, on the northern side of the island, and negative northward shear in zonal wind, counterclockwise vorticity and convergence, hence enhanced rainfall, on the southern side of the island. Incidentally, similar reasoning explains the observation that the southern coast of Jawa is climatologically wetter than the northern coast (not shown here).

[27] The features in the station observations data are not appropriately represented in coarse resolution data sets such as the satellite-gauge product of GPCP, or for that matter in general circulation models, as will be demonstrated in the next section. Such features may be indicative of predictability at a smaller scale and should be made the object of further investigation with high-resolution country-level meteorological data. A detailed description of the interaction between the large-scale and local circulation systems as influenced by land surface/topography is given by Qian et al. (manuscript in preparation, 2007), in the context of medium-resolution regional modeling simulations. In the work by Qian et al. (manuscript in preparation, 2007), initial results from a 30-year simulation run at 25 km resolution over Jawa are shown to reproduce these same features quite convincingly. Additional simulations with a purely dynamical version of the regional model indicate that it is the dry dynamical response in the interaction of the near-surface circulation with the land-ocean boundary that is responsible for the local divergent or convergent circulations that determine the rainfall anomalies during the core of the monsoon. Such simulations, in addition to allowing to test dynamical hypotheses by diagnosing the development of anomalies, also afford the opportunity to explore dynamical downscaling options for seasonal climate prediction in the region.

5. Tropical Tropospheric Temperature Adjustment to ENSO in an Atmospheric General Circulation Model

[28] In this final section we report on simulations with an atmospheric model that help elucidate the workings of the ENSO teleconnection to the Maritime continent in light of

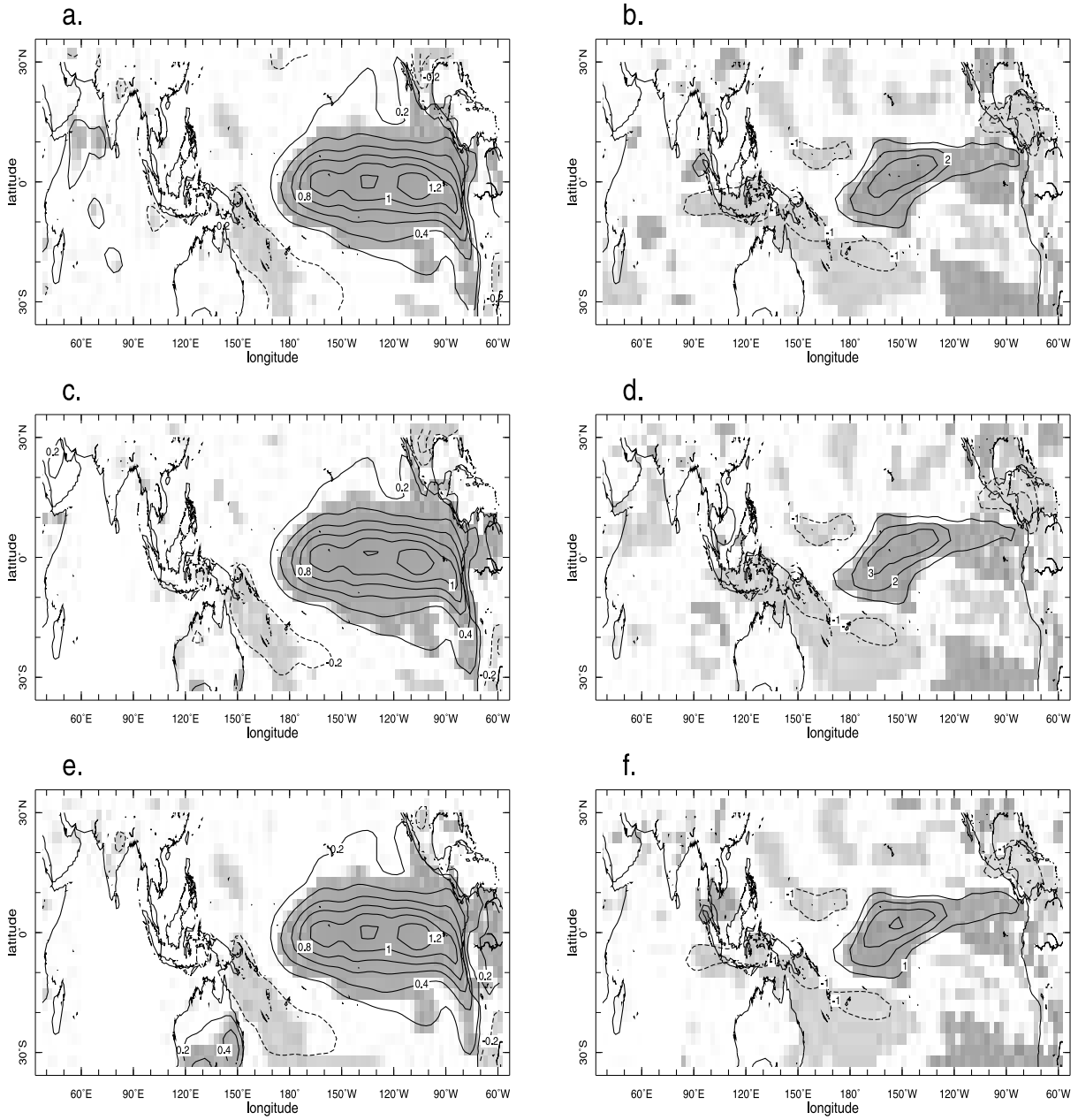

Figure 11. July–December(0) anomalies in (left) surface temperature and (right) precipitation in the (a and b) GOGA, (c and d) POGA, and (e and f) POGA-ML simulations with CCM3, during 1949–2004. Shading represents statistical significance of the anomalies at the 95% significance level. Contour is every 0.2°C (Figures 11a, 11c, and 11e) and every mm/day (Figures 11b, 11d, and 11f).

the tropical tropospheric temperature (TT) mechanism [*Chiang and Sobel*, 2002].

[29] We analyze output from simulations with CCM3, version 3 of NCAR's Community Climate Model [*Kiehl et al.*, 1998], in the version maintained at Lamont-Doherty Earth Observatory by R. Seager and colleagues. Ensembles of simulations with CCM3 were integrated in 3 model configurations. In two, known as GOGA (Global Ocean–Global Atmosphere) and POGA (Pacific Ocean–Global Atmosphere), SST, taken from *Kaplan et al.* [1997, 1998], was prescribed to vary monthly as observed: globally in GOGA, in the tropical Pacific only in POGA. SST was prescribed as observed in the entire geographical tropical Pacific basin (not shown), from the west coast of the Americas to the eastern Indian Ocean, with the Malay peninsula and the islands of Sumatera and Jawa delineating its western border. In POGA outside of the tropical Pacific SST was prescribed to follow a monthly varying climatology. In the third configuration, called POGA-ML, or POGA-Mixed Layer, SST was again prescribed to vary monthly as observed in the tropical Pacific only. Outside of it, it was prognosed using a two-layer entraining ocean model whose mixed layer depth is specified to vary according to observations seasonally, but not interannually, and

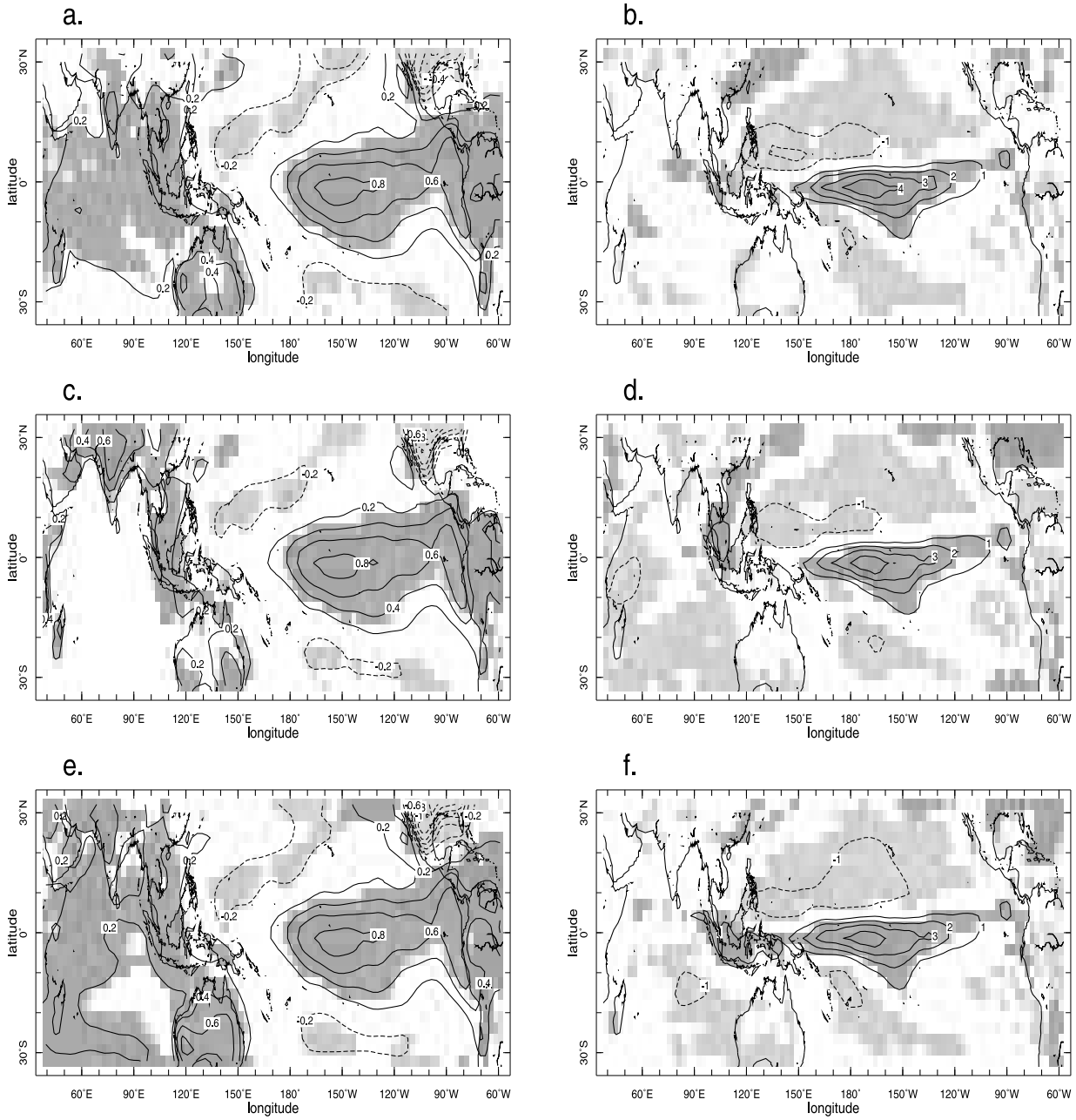

Figure 12. Same as in Figure 11 but for January–June(1).

which makes use of a q-flux correction in both layers to keep temperature from straying too far from climatology.

[30] Interpretation of Figures 11 and 12 summarizes our findings. In July–December(0) of warm ENSO years (Figure 11) CCM3 captures the atmospheric essence of the ENSO teleconnection. The warm SST anomalies in the tropical Pacific dominate, and force positive rainfall anomalies in this same source region, and negative anomalies elsewhere in the deep tropics, including over the Maritime continent (Figures 11b, 11d, and 11f). The coupled tropical ocean-atmosphere system is feeling ENSO's perturbation, and the warm tropical tropospheric temperature anomalies are making the atmosphere more stable, hence convection more difficult to trigger.

[31] By January–June(1) (Figure 12) the remote tropics have had time to adjust to ENSO; the Indian Ocean has warmed up, both in observations/GOGA (Figure 12a) and in POGA-ML (Figure 12e). In the GOGA framework, the widespread warming of the Indo-Pacific sector is associated with the absence of any significant anomalies in precipitation over monsoonal Indonesia (Figure 12b). This is consistent with cancellation of the effects of ENSO's direct atmospheric forcing, which imparts a drying tendency, and its indirect oceanic forcing, with the warming of the oceans favoring wet conditions. In POGA, it looks as if the

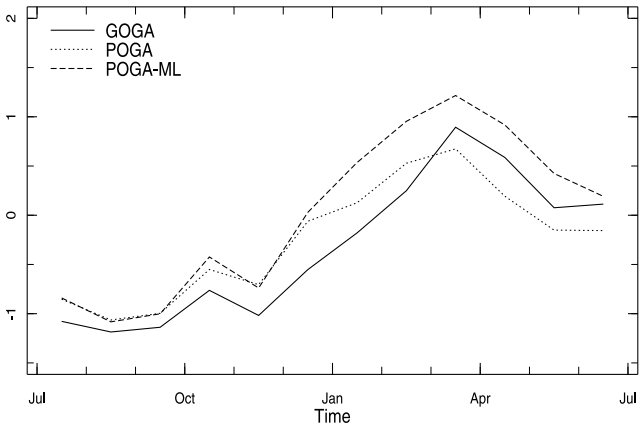

Figure 13. Average warm ENSO life cycle of anomalous rainfall averaged over a monsoonal Indonesia box, between 100°E and 140°E, 10°S and the equator, in GOGA (solid), POGA (dotted) and POGA-ML (dashed) (in mm/day).

localized warming, confined to a narrow longitudinal strip between Sumatera and Kalimantan, may be responsible for setting up zonal gradients in SST which favor convergence of the near-surface flow toward the warm SST anomaly, hence positive rainfall anomalies locally, over northern portions of Sumatera and the Malay peninsula (Figure 12d).

[32] In POGA-ML (Figures 12e and 12f) only has the adjustment of the remote ocean-atmosphere occurred in an internally consistent way. As hypothesized by *Chiang and Sobel* [2002], in regions of climatological deep convection the ENSO-related tropical tropospheric temperature anomaly is communicated all the way to the surface by means of anomalous surface fluxes. Rainfall anomalies, specifically anomalies across monsoonal Indonesia, are not simply directly forced by SST anomalies, otherwise we would expect them to be similar in GOGA and in POGA-ML. The fact that rainfall anomalies are coherent and significant in POGA-ML but not in GOGA is indication that they are intrinsic to the way in which the ocean-atmosphere system adjusts to a different state, one where the warmer surface is capable of sustaining stronger convection. The global model does not resolve the complexity of the geography of the region, hence it cannot reproduce the smaller-scale features in the rainfall response described in Figures 9c and 9d. However, it is consistent with the general explanation that invokes adjustment to a new equilibrium, a warmer, moister state in the case of warm ENSO, in which features of the local circulation interact with the large scale to produce the observed patterns.

[33] The difference in the response to warm ENSO forcing in monsoonal Indonesia rainfall in the 3 simulations is depicted in Figure 13, the July(0)–June(1) life cycle of rainfall anomalies averaged over the domain between 100°E and 140°E, 10°S and the equator. From July(0) to November(0), all setups reproduce negative rainfall anomalies. These are more pronounced in GOGA, possibly because the separate effects of remote and local SSTs add up. December(0) is when the setups start to diverge. As expected, the turnaround to positive rainfall anomalies is most abrupt and pronounced in the POGA-ML simulation, where the adjustment to new equilibrium conditions occurs in a dynamically coupled way.

6. Conclusions

[34] The climate of Indonesia is shaped by ENSO. The geophysical configuration of the coupled ocean-atmosphere system of the Indo-Pacific region is such that precipitation is normally favored over the Western Pacific warm pool, while the eastern and central equatorial Pacific and western Indian Oceans experience an overall drier climate [*Cane and Molnar*, 2001]. This configuration is strongly perturbed by the occurrence of warm ENSO events every 3 to 7 years. This occurrence is of great consequence for the ecosystems of the region, natural and anthropogenic alike; canopy tree recruitment in Kalimantan [*Curran et al.*, 1999], rice production in Jawa [*Kirono et al.*, 1999; *Naylor et al.*, 2001], and forest fires in Kalimantan [*Siegert et al.*, 2001] are but a few examples of ENSO's broader impacts on ecosystem function/services in the broader Maritime continent region.

[35] In this study, we reviewed the physical basis for predictability of climate over Indonesia, and demonstrated how such predictability hinges on the development of ENSO anomalies in the ocean-atmosphere system. The development of ENSO teleconnections is such that predictability of rainfall in Indonesia, especially in the monsoonal regions of Indonesia, is high during the dry and transition seasons into the rainy season. An analysis of the large-scale mechanisms involved and preliminary results from analyses with statistical and dynamical downscaling techniques, as well as analyses of atmospheric model simulations suggest that these anomalies are consistent with adjustment of the deep tropical climate system to tropospheric temperature (TT) anomalies.

[36] We also identified two directions for improvement in the quantitative assessment of predictability and its application. At large spatial scales, we showed that because of the intrinsically coupled nature of ENSO, and of tropical climate, a simple one-tier prediction system, composed of an atmospheric model coupled to a two-layer thermodynamic ocean model, better captures the dynamics inherent to the development of the ENSO teleconnection than a two-tier system, i.e., one in which SST anomalies are predicted first, and then used to force the atmospheric response. This conclusion echoes the work of *Wu and Kirtman* [2005], *Krishna Kumar et al.* [2005], *Wang et al.* [2005], and *Bracco et al.* [2007], who focused on the ENSO teleconnection to the South Asian monsoon. At intermediate spatial scales, i.e., scales that are neither those of coarse resolution products such as GPCP, or of global atmospheric models, nor the very small scales of a specific locality, we found promise in the identification of predictable structures. Specifically, we found that a dipolar structure between the northern and southern coasts of Jawa is associated with ENSO both statistically and dynamically. These intermediate spatial scales connect locations that are differentially affected by the same phenomenon, hence their consideration has potential practical consequences. They should be considered when upscaling the application of climate information, e.g., from the management of tail-end rice production

in one district of Jawa Barat to livelihood systems across the entire island.

[37] **Acknowledgments.** We thank David Battisti, John Chiang, Brad Lyon, Vincent Moron, Rizaldi Boer and his students at Institut Pertanian Bogor for sharing their knowledge and insight. We thank three anonymous reviewers for their insightful comments. We also thank Richard Seager, Gustavo Correa and Naomi Naik for integrating and sharing their atmospheric model simulations with CCM3. We are grateful to the U.S. Agency for International Development's Office of Foreign Disaster Assistance (grant DFD-A-00-03-00005-00) and NOAA's Office of Global Programs (grant NA07GP0213) for their financial support.

References

Aldrian, E., and R. D. Susanto (2003), Identification of three dominant rainfall regions within Indonesia and their relationship to sea surface temperature, *Int. J. Climatol.*, *23*, 1435–1452.

Aldrian, E., L. Dümenil-Gates, and F. H. Widodo (2007), Seasonal variability of Indonesian rainfall in ECHAM4 simulations and in the reanalyses: The role of ENSO, *Theor. Appl. Climatol.*, *87*, 41–59, doi:10.1007/s00704-006-0218-8.

Bracco, A., F. Kucharski, F. Molteni, W. Hazeleger, and C. Severijns (2005), Internal and forced modes of variability in the Indian Ocean, *Geophys. Res. Lett.*, *32*, L12707, doi:10.1029/2005GL023154.

Bracco, A., F. Kucharski, F. Molteni, W. Hazeleger, and C. Severijns (2007), A recipe for simulating the interannual variability of the Asian summer monsoon and its relationship to ENSO, *Clim. Dyn.*, *28*, 441–460, doi:10.1007/s00382-006-0190-0.

Cane, M. A., and P. Molnar (2001), Closing of the Indonesian seaway as a precursor to east African aridification around 34 million years ago, *Nature*, *411*, 157–162, doi:10.1038/35075500.

Chang, C.-P. (2005), The Maritime continent monsoon, in *The Global Monsoon System: Research and Forecast*, edited by C.-P. Chang, B. Wang, and N.-C. Lau, *WMO/TD 1266*, pp. 387–404, World Meteorol. Organ., Geneva, Switzerland.

Chang, C.-P., Z. Wang, J. Ju, and T. Li (2004), On the relationship between Western Maritime continent monsoon rainfall and ENSO during Northern winter, *J. Clim.*, *17*, 665–672, doi:10.1175/1520-0442(2004)017.

Chiang, J. C. H., and B. R. Lintner (2005), Mechanisms of remote tropical surface warming during El Niño, *J. Clim.*, *18*, 4130–4149, doi:10.1175/JCLI3529.1.

Chiang, J. C. H., and A. H. Sobel (2002), Tropical tropospheric temperature variations caused by ENSO and their influence on the remote tropical climate, *J. Clim.*, *15*, 2616–2631.

Curran, L. M., I. Caniago, G. D. Paoli, D. Astianti, M. Kusneti, M. Leighton, C. E. Nirarita, and H. Haeruman (1999), Impact of El Niño and logging on canopy tree recruitment in Borneo, *Science*, *286*, 2184–2188.

Glantz, M. H., R. W. Katz, and N. Nicholls (1991), *Teleconnections Linking Worldwide Climate Anomalies*, 535 pp., Cambridge Univ. Press, New York.

Hackert, E. C., and S. Hastenrath (1986), Mechanisms of Java rainfall anomalies, *Mon. Weather Rev.*, *114*, 745–757.

Harger, J. R. E. (1995), ENSO variations and drought occurrence in Indonesia and the Philippines, *Atmos. Environ.*, *29*, 1943–1955.

Haylock, M., and J. McBride (2001), Spatial coherence and predictability of Indonesian wet season rainfall, *J. Clim.*, *14*, 3882–3887.

Hendon, H. H. (2003), Indonesian rainfall variability: Impacts of ENSO and local air-sea interaction, *J. Clim.*, *16*, 177–1790.

Hoerling, M. P., A. Kumar, and M. Zhong (1997), El Niño, La Niña, and the nonlinearity of their teleconnections, *J. Clim.*, *10*, 1769–1786.

Huffman, G. J., R. F. Adler, P. Arkin, A. Chang, R. Ferraro, A. Gruber, J. Janowiak, A. McNab, B. Rudolf, and U. Schneider (1997), The global precipitation climatology project (GPCP) combined precipitation dataset, *Bull. Am. Meteorol. Soc.*, *78*, 5–20.

Kalnay, E., et al. (1996), The NCEP-NCAR 40-year reanalysis project, *Bull. Am. Meteorol. Soc.*, *77*, 437–471.

Kaplan, A., Y. Kushnir, M. A. Cane, and M. B. Blumenthal (1997), Reduced space optimal analysis for historical data sets: 136 years of Atlantic sea surface temperatures, *J. Geophys. Res.*, *102*, 27,835–27,860.

Kaplan, A., M. A. Cane, Y. Kushnir, A. C. Clement, M. B. Blumenthal, and B. Rajagopalan (1998), Analyses of global sea surface temperature 1856–1991, *J. Geophys. Res.*, *103*, 18,567–18,589.

Kiehl, J. T., J. J. Hack, G. B. Bonan, B. A. Boville, D. L. Williamson, and P. J. Rasch (1998), The National Center for Atmospheric Research Community Climate Model: CCM3, *J. Clim.*, *11*, 1131–1149.

Kirono, D. G. C., N. J. Tapper, and J. L. McBride (1999), Documenting Indonesian rainfall in the 1997–1998 El Niño event, *Phys. Geogr.*, *20*, 422–435.

Klein, S. A., B. Soden, and N.-C. Lau (1999), Remote sea surface temperature variations during ENSO: Evidence for a tropical atmospheric bridge, *J. Clim.*, *12*, 917–932.

Krishna Kumar, K., M. P. Hoerling, and B. Rajagopalan (2005), Advancing dynamical prediction of Indian monsoon rainfall, *Geophys. Res. Lett.*, *32*, L08704, doi:10.1029/2004GL021979.

Lintner, B. R., and J. C. H. Chiang (2007), Adjustment of the remote tropical climate to El Niño conditions, *J. Clim.*, *20*, 2544–2557.

McBride, J. L., M. R. Haylock, and N. Nicholls (2003), Relationships between the Maritime Continent heat source and the El Niño–Southern Oscillation phenomenon, *J. Clim.*, *16*, 2905–2914.

Mo, K. C., and R. W. Higgins (1998), The Pacific–South American modes and tropical convection during the Southern Hemisphere winter, *Mon. Weather Rev.*, *126*, 1581–1596.

Murtugudde, R., J. P. J. McCreary, and A. J. Busalacchi (2000), Oceanic processes associated with anomalous events in the Indian Ocean with relevance to 1997–1998, *J. Geophys. Res.*, *105*(C2), 3295–3306.

Naylor, R. L., W. P. Falcon, D. Rochberg, and N. Wada (2001), Using El Niño–Southern Oscillation climate data to predict rice production in Indonesia, *Clim. Change*, *50*, 255–265.

Neelin, J. D., D. S. Battisti, A. C. Hirst, F.-F. Jin, Y. Wakata, T. Yamagata, and S. E. Zebiak (1998), ENSO theory, *J. Geophys. Res.*, *103*, 14,261–14,290.

Park, S., and C. B. Leovy (2004), Marine low-cloud anomalies associated with ENSO, *J. Clim.*, *17*, 3448–3469.

Rasmusson, E. M., and T. H. Carpenter (1982), Variations in tropical sea surface temperature and surface wind fields associated with the Southern Oscillation/El Niño, *Mon. Weather Rev.*, *110*, 354–384.

Ropelewski, C. F., and M. S. Halpert (1987), Global and regional precipitation patterns associated with the El Niño/Southern Oscillation, *Mon. Weather Rev.*, *115*, 1606–1626.

Ropelewski, C. F., and M. S. Halpert (1989), Precipitation patterns associated with the high index phase of the Southern Oscillation, *J. Clim.*, *2*, 268–284.

Saravanan, R., and P. Chang (2000), Interaction between tropical Atlantic variability and El Niño–Southern Oscillation, *J. Clim.*, *20*, 2177–2194.

Siegert, F., G. Ruecker, A. Hinrichs, and A. A. Hoffman (2001), Increased damage from fires in logged forests during droughts caused by El Niño, *Nature*, *414*, 437–440.

Su, H., and J. D. Neelin (2002), Teleconnection mechanisms for tropical Pacific descent anomalies during El Niño, *J. Atmos. Sci.*, *59*, 2694–2712.

Su, H., J. D. Neelin, and J. E. Meyerson (2005), Mechanisms for lagged atmospheric response to ENSO SST forcing, *J. Clim.*, *18*, 4195–4215.

Susanto, R. D., A. L. Gordon, and Q. Zheng (2001), Upwelling along the coasts of Java and Sumatra and its relation to ENSO, *Geophys. Res. Lett.*, *28*(8), 1599–1602.

Vose, R. S., R. L. Schmoyer, P. M. Steurer, T. C. Peterson, R. Heim, T. R. Karl, and J. Eischeid (1992), The Global Historical Climatology Network: Long-term monthly temperature, precipitation, sea level pressure, and station pressure data, *ORNL/CDIAC-53, NDP-041*, 300 pp., Carbon Dioxide Inf. Anal. Cent., Oak Ridge Natl. Lab., Oak Ridge, Tenn.

Wallace, J. M., and D. S. Gutzler (1981), Teleconnections in the geopotential height field during the Northern Hemisphere winter, *Mon. Weather Rev.*, *109*, 784–812.

Wallace, J. M., E. M. Rasmusson, T. P. Mitchell, V. E. Kousky, E. S. Sarachik, and H. von Storch (1998), On the structure and evolution of ENSO-related climate variability in the tropical Pacific: Lessons from TOGA, *J. Geophys. Res.*, *103*(C7), 14,241–14,259.

Wang, B., Q. Ding, X. Fu, I.-S. Kang, K. Jin, J. Shukla, and F. Doblas-Reyes (2005), Fundamental challenge in simulation and prediction of summer monsoon rainfall, *Geophys. Res. Lett.*, *32*, L15711, doi:10.1029/2005GL022734.

Wijffels, S., and G. Meyers (2004), An intersection of oceanic waveguides: Variability in the Indonesian Throughflow region, *J. Phys. Oceanogr.*, *34*, 1232–1253.

Wu, R., and B. P. Kirtman (2005), Roles of Indian and Pacific Ocean air-sea coupling in tropical atmospheric variability, *Clim. Dyn.*, *25*, 155–170, doi:10.1007/s00382-005-0003-x.

Yulaeva, E., and J. M. Wallace (1994), The signature of ENSO in global temperature and precipitation fields derived from the microwave sounding unit, *J. Clim.*, *7*, 1719–1736.

A. Giannini, J.-H. Qian, and A. W. Robertson, International Research Institute for Climate and Society, 61 Rt 9W, Palisades, NY 10964-8000, USA. (alesall@iri.columbia.edu)